Int J Wireless Inf Networks (2012) 19:229–238
DOI 10.1007/s10776-012-0193-1

Accuracy of RSS-Based RF Localization in Multi-capsule Endoscopy

Yunxing Ye · Pranay Swar · Kaveh Pahlavan · Kaveh Ghaboosi

Received: 23 January 2012 / Accepted: 2 August 2012 / Published online: 18 August 2012

Abstract In this paper, we derive and analyze cooperative localization bounds for endoscopic wireless capsule as it passes through the human gastrointestinal (GI) tract. We derive the Cramer-Rao bound (CRB) variance limits on location estimators which use measured received signal strength (RSS). Using a three-dimension human body model from a full wave simulation software and log-normal models for RSS propagation from implant organs to body surface, we calculate bounds on location estimators in three digestive organs: stomach, small intestine and large intestine. We provide analysis of the factors affecting localization accuracy, including various organ environments, external sensor array topology, number of pills in cooperation and the random variations in transmit power of sensor nodes. We also do localization accuracy analysis for the case when transmit power of the sensor is random with known priori distribution. The simulation results show that the number of receiver sensors on body surface has more influence on the accuracy of localization than the number of pills in cooperation inside the GI tract, The large intestine is affected the most with the transmit power randomness.

Y. Ye (✉) · P. Swar · K. Pahlavan · K. Ghaboosi
Center for Wireless Information, Network Studies, Worcester Polytechnic Institute, Worcester, MA 01609, USA
e-mail: abusedna@gmail.com; yunxingye@wpi.edu

P. Swar
e-mail: pranay.swar@wpi.edu

K. Pahlavan
e-mail: kaveh@wpi.edu

K. Ghaboosi
e-mail: kavehg@wpi.edu

Keywords Endoscopy capsule · RSS localization · Cramer-Rao bound · 3D · Cooperative localization · Power randomness

1 Introduction

Recently, wireless capsule endoscopy (WCE) has attracted lots of attention due to its non-invasive nature. Examination of the gastro-intestinal (GI) track is necessary to identify any colorectal cancer inside the digestive system tube. It has been shown that colorectal cancer has been the second leading cause of cancer-related deaths in USA. Furthermore, WCE allows the physician to visualize the entire GI tract without scope trauma and air insufflations. Traditional techniques such as gastroscopy and colonoscopy can only reach the first few or last several feet of the GI tract. The WCE received its approval from the U.S. Food and Drug Administration (FDA) in 2001, and more than 200,000 patients have enjoyed the benefits of this new technology. WCE starts with the patient swallowing the capsule. The natural peristalsis moves the capsule smoothly and painlessly throughout the GI track, which is transmitting color images taken by the camera in the capsule as it passes. The procedure is ambulatory allowing the patients to continue with their daily activities throughout the endoscopic examinations. Despite the advantages the WCE have, it is reported that a physician spends one or two hours to assess the photos taken during each WCE examination, since approximately fifty thousands photos are taken during the eight hours period of examination [1]. This slows down the process of examination and increases the cost of the procedure significantly. Meanwhile, after the examination by WCE, the physician may want to revisit the sites of interest for further diagnosis or treatment. Accurate location information of the capsule can help in both reducing the time needed for

assessing the photos and assisting the physicians for follow-up interventions.

Various technologies for localization of the capsule have been explored in feasibility studies. The original idea is to use a spatially scanning system to locate the points with the strongest RSS. The system is non-commercial and cumbersome. Frisch et al. [2] developed a RF triangulation system using an external sensor array that measures signal strength of capsule transmissions at multiple points and uses this information to estimate the distance. The average experimental error is reported to be 37.7 mm [3]. Kuth et al. [4] proposed a method for determining the position of and orientation of the capsule by means of X-ray radiation image processing. In this case, the capsule can be seen unambiguously since it has a multiplicity of radiation-opaque elements which are usually metallic or plastic and show a very clear image. Thus, it is possible to operate with an extremely low radiation dose in order to reduce the health risks on the patients. Kawasaki [5] disclosed a method for finding the location of medical implant devices by using the time of arrival (TOA) based pattern recognition method. First, the propagation speed of signal inside human body is estimate by processing the images from CT or MRI system. Then, an adaptive template synthesis method is applied to calculate the propagation time based on the output of the correlator between the transmitter and the receiver. Other techniques developed for capsule localization include magnetic field sensing [6]. A small permanent magnet is enclosed into the capsule. With the sensing data of magnetic sensor array outside the patient's body, the 3D location and 2D orientation of the capsule are estimated. Inertial system has also been used for capsule localization [7]. In this work, a 3×3 mm digital triaxial accelerometer, which operates at 20 Hz, was integrated within the capsule and data was transmitted over Zigbee technology to an external computer. Since the acceleration is directly measured, velocity can be obtained more accurately than position because it requires only a single integration. Since identifying the physical location of each capture of capsule photo is important in both diagnostic and therapeutic applications of WCEs.

Among these technologies, RF signal based localization systems have the advantage of application-non-specific and relatively low cost for implementation. Therefore, it has been chosen for use with the Smartpill capsule [8] in USA and the M2A capsule [9] in Israel. Generally, the RF localization technique is based on TOA, angle of arrival (AOA) or received signal strength (RSS) measurements. A widely known benefit of TOA based techniques is their high accuracy compared to RSS and AOA based techniques. However, the strong absorption of human tissue causes large errors in TOA estimation and the limited bandwidth (402–405 MHz) of the Medical Implant Communication Services (MICS) band prevent us from high resolution TOA estimation. The problem is made even worse by the GI movement, and the filling and emptying cycle, resulting in unpredictable ranging error [10]. Thus, the ranging information from TOA estimation is not promising with the current technology.

The RSS based techniques are less sensitive to bandwidth limitation and harsh propagation environment. There are basically two ways to use the RSS information for localization, triangulation and pattern recognition. In this paper, we only address the issues related to RSS triangulation techniques. RSS Triangulation technique is based on the path loss model from implant tissues to body surface. The model is used to calculate the distance between each external sensor and the capsule, then at least four link distances are used to calculate the location of the capsule in 3D space.

The most challenge problem in capsule localization comes from the complexity of the environment where the capsule travels through. Since the GI tract is a long tubular structure that folds upon itself many times and is free to move within the abdominal cavity, it is very difficult to accurately localize the capsule. Meanwhile, due to the activities of patient and body passive motions such as respiration, the absolute location of sensors on the surface of the body and their relative positions to the capsule inside body keep varying, making the definition of localization different from traditional scenarios. Currently, most of the researchers have focused on developing the algorithms and mathematical models for solving the triangulation problem [3, 11]. In this paper, we take a different approach. Based on the statistical implant path loss model developed in [12], we focus on the accuracy possible for capsules in the GI tract using RSS based triangulation technique, Yi et al. have developed the localization bound calculation for single pill situation in [13]. The Cramer-Rao bound (CRB) presented in this paper quantify the limits of localization accuracy with certain reference-points topology, implant path loss model and number of pills in cooperation. Our aim is to analyze the accuracy achievable at various organs and determine if the accuracies are enough for endoscopy applications. Similar works have been done for indoor geolocation applications [14] and robot localization applications [15].

We begin in Sect. 2 by summarizing the performance evaluation methodology which includes the scenario description and the implant to body surface path loss model for GI tract environment. Next, using the coordinates value from scenario and the path loss model, we derive the CRB for cooperative capsule localization and the localization bound with randomness in the transmitted power in Sect. 3. In Sect. 4, we provide results of simulation which highlight the network and organ location parameters that affect the localization accuracy. Finally, we conclude the paper in Sect. 5.

2 Performance Evaluation Methodology

2.1 Performance Evaluation Scenario

The GI tract consists of the esophagus, stomach, small intestine, and large intestine, as shown in Fig. 1. In order to create a simulation scenario for calculating the CRB of wireless capsule as it travels through the human digestive system, we use a 3D human model from the three-dimensional full-wave electromagnetic field simulation system (Ansoft [16]). The 3D human body model has a spatial resolution of 2 mm and includes frequency dependent dielectric properties of 300+ parts in a male human body. We extract the 3D coordinates of digestive organs from the human body model, which is illustrated in Fig. 2.

For the design of the topology of receiver sensors on body surface, we followed the idea in [2], assuming the receiver arrays are placed on a jacket wared by the patient during the examination. Same number of receivers are fixed in front and on the back of the jacket. We calculated the CRB for 8, 16, 32 and 64 receiver sensors with a three dimensional range of 268 × 323 × 312 mm, a typical network topology for 32 receiver sensors is illustrated in Fig. 3.

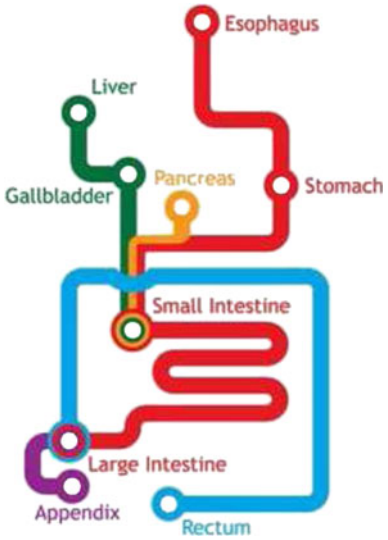

Fig. 1 A schematic of the GI tract. The typical path of a WCE is along the red and blue line (Color figure online)

2.2 Path Loss Model for GI Tract Environment

In this section, we describe the statistical implant to body surface path loss model which is used for calculating the CRB of WCE localization. The model was developed by National Institute of Standards and Technology (NIST) at MICS band [12]. The main components used for developing the model include: a three-dimensional human body model, the propagation engine which is a three-dimensional full wave electromagnetic field simulator, the 3D immersive and visualization platform and implantable antenna.

The path loss in dB at some distance d between the transmitter and receiver can be statistically modeled by the following equation:

$$L_p(d) = L_p(d_0) + 10\alpha \log_{10}(d/d_0) + S(d > d_0) \quad (1)$$

where d_0 is the reference distance (i.e. 50 mm), and α is the path loss gradient which is determined by the propagation environment. For example, in free space, $\alpha = 2$. As we already mentioned, human body tissue strongly absorbs RF signal. Therefore, much higher value for the path loss gradient is expected. S is a random variable log-normally distributed around the mean which represents the deviation caused by shadowing effect of human tissue.

The parameters of the implant to body surface path loss model are summarized in Table 1.

In Table 1 σ_{dB} is the standard deviation of shadow fading S. Note that there are two sets of parameters for path loss from deep and near surface implant to body surface. During our

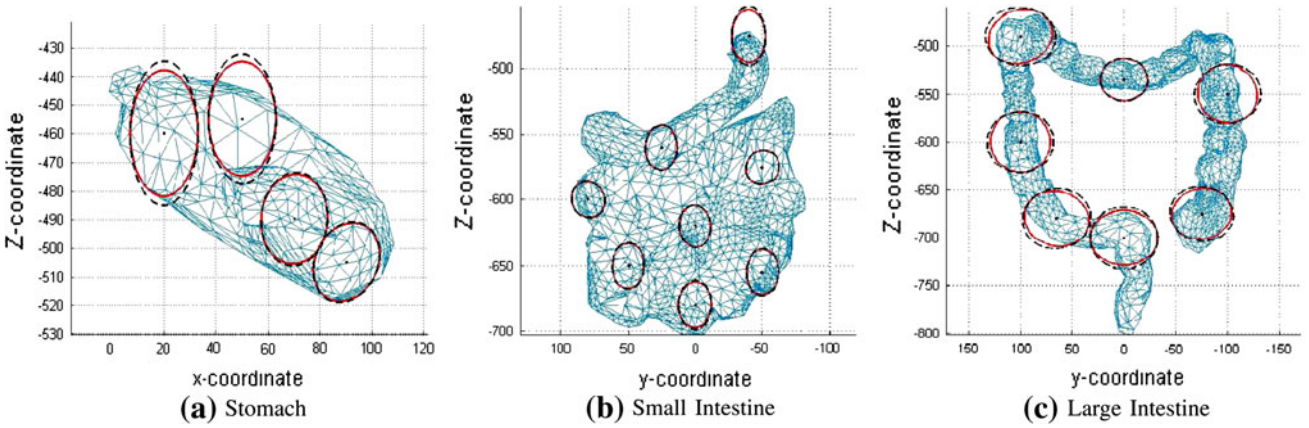

Fig. 2 Comparison of CRB on $1 - \sigma$ uncertainty ellipses. When transmitted power are perfectly known (*solid line in red*) or random with $\sigma_\pi = 10$ dB (*sashed lines in black*), for different unknown capsule locations (Color figure online)

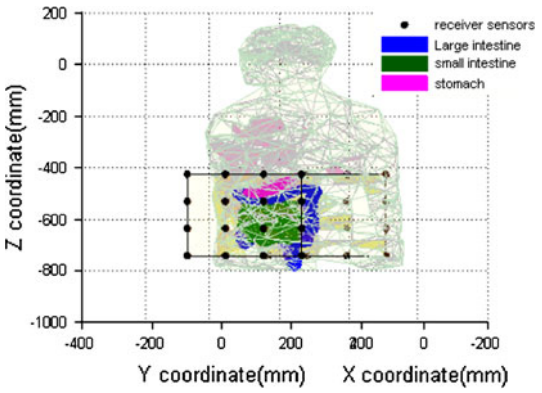

Fig. 3 WCE cooperative localization scenario

Table 1 Parameters for the statistical implant to body surface path loss model

Implant to body surface	$L_p(d_0)$ (dB)	α	σ_{dB}
Deep tissue	47.14	4.26	7.85
Near surface	49.81	4.22	6.81

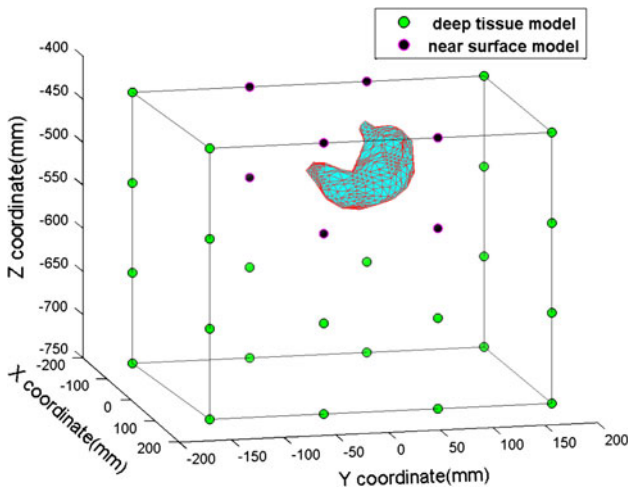

Fig. 4 Path loss model selection (32 receiver sensors, stomach)

simulation, we use 10 cm distance between the transmitter and receiver on body surface as the threshold for choosing the model. If the distance is less than 10 cm, we use the near surface to surface path loss model, otherwise the deep tissue to surface model is used, One illustration of how we select the models for various receiver sensors shown in Fig. 4.

2.3 Randomness in Transmit Power

In realistic sensor networks, the sensors do not know their precise transmitted power level due to cost of the device calibration. Although, they may report that the transmitted power is at a particular level, the actual power transmitted varies by few dBs about this nominal value [17]. The major factors that causes transmitted power variance for body area networks are listed as follows: (a) device manufacturing variation and battery level variation from sensor to sensor, (b) movement of the human body due to locomotion and changes in the orientation of the antenna, (c) the sensor antennas might not be at the same distance from the human body surface at a given time. Some antennas might be touching the body while others might be few mm's away from the body. As reported in [18], antenna touching the body has a lower gain than the antenna 15 mm away from the body. All these factors contribute to the randomness in the transmitted power which affects the localization accuracy.

3 CRB for 3D Capsule Localization

In this section, we derive the 3D CRB based on the path loss model discussed in the previous section. We consider both situations where multiple capsules are in cooperation and when there is randomness in power. The CRB for 2D localization bounds has been derived in [19]. Here, we derive the bounds in three dimensions by extending the results obtained in two dimensions.

3.1 CRB for Multicapsule Cooperative Localization

Based on the path loss model in Sect. 2, we derive the 3D CRB for cooperative localization in WCE. The scenario we consider is as follows, N wireless endoscopic capsules are distributed in the digestive system with location given by $\theta_c = [p_1, \ldots, p_N]$. These pills are blindfolded devices but they can measure the RSS from each other and transmit the information out to the receiver array for further processing. M receiver sensors are placed on the surface of the human body with location given by $\theta_r = [p_{N+1}, \ldots, p_{N+M}]$. The vector of device parameters is $\theta = [\theta_c\ \theta_r]$. For this three dimensional system, $p_i = [x_i, y_i, z_i]^T$, where $i \in [1, N+M]$ and T is the transpose operation. The unknown parameters to be estimated can be represented by a $3 \times N$ coordinates matrix.

$$\theta_c = [p_1, p_2, \ldots, p_N] = \begin{bmatrix} x_1 & x_2 & \ldots & x_N \\ y_1 & y_2 & \ldots & y_N \\ z_1 & z_2 & \ldots & z_N \end{bmatrix} \tag{2}$$

Consider devices (devices include capsules and receivers) i and j make pair-wise observations $X_{i,j}$. We assume each receiver sensor can measure the RSS from all the capsules inside the body, but the path loss parameters for different links varies as the distance between the receiver sensor and capsule inside the body changes. Therefore, Let $H(i) = \{j$: device j makes pair-wise observations with device $i\}$. $H\{i\} = \{1, \ldots i-1, i+1, \ldots N+M\}$ for $i \in [1, N]$ and $H\{i\} = \{1, \ldots N\}$ for $i \in [N+1, N+M]$ because a device cannot make pairwise

observation with itself and the receivers do not make observations with receivers either. Therefore the length of the observation vector X is $N \times (N + M - 1) + M \times N$.

By reciprocity, we assume $X_{i,j} = X_{j,i}$; thus, it is sufficient to consider only the lower triangle of the observation matrix X when formulating the joint likelihood function [20]. The CRB on the covariance matrix of any unbiased estimator $\hat{\theta}$ is given by [21]:

$$cov(\hat{\theta}) = E\left[(\hat{\theta} - \theta)(\hat{\theta} - \theta)^T\right] \geq F_\theta^{-1} \tag{3}$$

where $E[\cdot]$ is the expectation operation and F is the Fisher information matrix (FIM) defined as:

$$\begin{aligned} F_\theta &= -E\nabla_\theta(\nabla_\theta \ln f(X|\theta))^T \\ &= E_\theta\left[\frac{\partial}{\partial\theta}\ln f(X|\theta)\left(\frac{\partial}{\partial\theta}\ln f(X|\theta)\right)^T\right] \\ &= \begin{bmatrix} F_{Rxx} & F_{Rxy} & F_{Rxz} \\ F_{Rxy}^T & F_{Ryy} & F_{Ryz} \\ F_{Rxz}^T & F_{Ryz}^T & F_{Rzz} \end{bmatrix} (\text{3D situation}) \end{aligned} \tag{4}$$

where $f(X|\theta)$ is the joint PDF of the observation vector X conditioned on θ. For the RSS measurements case, the $X_{i,j}$ are log-normal random variables, and the density is given by [19]

$$\begin{aligned} f(X_{i,j}|p_i, p_j) &= \frac{10/\log 10}{\sqrt{2\pi\sigma_{\text{dB}}^2}}\frac{1}{X_{i,j}}\exp\left[-\frac{b}{8}\left(\log\frac{d_{i,j}^2}{\tilde{d}_{i,j}^2}\right)^2\right] \\ b &= \left(\frac{10\alpha}{\sigma_{\text{dB}}}\right)^2 \\ \tilde{d}_{i,j} &= d_0\left(\frac{X_0}{X_{i,j}}\right)^{\frac{1}{\alpha}} \\ d_{i,j} &= \sqrt{(x_i - x_j)^2 + (y_i - y_j)^2 + (z_i - z_j)^2} \end{aligned} \tag{5}$$

for $i = 1, 2, \ldots, N + M$ and $j \in H(i), \tilde{d}(i,j)$ is the MLE of range $d_{i,j}$ given received power $X_{i,j}$. Then the logarithm of the joint condition pdf is:

$$l(X|\theta) = \sum_{i=1}^{M+N}\sum_{j\in Hij<i} \log f_{X|\theta}(X_{i,j}|p_i, p_j) \tag{6}$$

It is shown in [19] that the second partial derivative of (6) w.r.t θ_r and θ_s will be a summation of terms if θ_r and θ_s are coordinates of the same device k, but will be only one term if θ_r and θ_s are coordinates of different devices k and l, $k \neq l$. For example:

$$\begin{aligned} \frac{\partial^2 l(X|\theta)}{\partial x_k \partial z_k} &= -b\sum_{i\in H(k)}\frac{(x_i - x_k)(z_i - z_k)}{d_{i,k}^4}\left[-\log\frac{d_{i,k}^2}{\tilde{d}_{i,k}^2} + 1\right] \\ \frac{\partial^2 l(X|\theta)}{\partial x_k \partial z_l} &= -bI_{H(k)}(l)\frac{(x_i - x_k)(z_i - z_k)}{d_{i,k}^4}\left[\log\frac{d_{i,k}^2}{\tilde{d}_{i,k}^2} - 1\right] \end{aligned} \tag{7}$$

where $I_{H(k)}$ $(l) = 1$ if $l \in H(k)$ and 0 otherwise. Since $E\left(\frac{d_{i,k}^2}{\tilde{d}_{i,k}^2}\right) = 0$. Thus, the elements of F_θ are:

$$[F_{R_{xx}}]_{k,l} = \begin{cases} b\sum_{i\in H(k)}\frac{(x_k - x_i)^2}{d_{ki}^4} & k = l \\ -bI_{H(k)}(l)\frac{(x_k - x_l)^2}{d_{kl}^4} & k \neq l \end{cases} \tag{8}$$

$$[F_{R_{xy}}]_{k,l} = \begin{cases} b\sum_{i\in H(k)}\frac{(x_k - x_i)(y_k - y_i)}{d_{ki}^4} & k = l \\ -bI_{H(k)}(l)\frac{(x_k - x_l)(y_k - y_l)}{d_{kl}^4} & k \neq l \end{cases}$$

$$[F_{R_{xz}}]_{k,l} = \begin{cases} b\sum_{i\in H(k)}\frac{(x_k - x_i)(z_k - z_i)}{d_{ki}^4} & k = l \\ -bI_{H(k)}(l)\frac{(x_k - x_l)(z_k - z_l)}{d_{kl}^4} & k \neq l \end{cases}$$

$$[F_{R_{yy}}]_{k,l} = \begin{cases} b\sum_{i\in H(k)}\frac{(y_k - y_i)^2}{d_{ki}^4} & k = l \\ -bI_{H(k)}(l)\frac{(y_k - y_l)^2}{d_{kl}^4} & k \neq l \end{cases}$$

$$[F_{R_{yz}}]_{k,l} = \begin{cases} b\sum_{i\in H(k)}\frac{(y_k - y_i)(z_k - z_i)}{d_{ki}^4} & k = l \\ -bI_{H(k)}(l)\frac{(y_k - y_l)(z_k - z_l)}{d_{kl}^4} & k \neq l \end{cases}$$

$$[F_{R_{zz}}]_{k,l} = \begin{cases} b\sum_{i\in H(k)}\frac{(z_k - z_i)^2}{d_{ki}^4} & k = l \\ -bI_{H(k)}(l)\frac{(z_k - z_l)^2}{d_{kl}^4} & k \neq l \end{cases}$$

Let $\hat{x}_i, \hat{y}_i, \hat{z}_i$ be the unbiased estimation of x_i, y_i, z_i, the trace of the covariance of the ith location estimate is given by:

$$\begin{aligned} \sigma_i^2 &= tr\{cov_\theta(\hat{x}_i, \hat{y}_i, \hat{z}_i)\} \\ &= Var_\theta(\hat{x}_i) + Var_\theta(\hat{y}_i) + Var_\theta(\hat{z}_i) \\ &\geq \left[F_{R_{xx}} - (F_{R_{xy}}F_{R_{xz}})\begin{pmatrix} F_{R_{yy}} & F_{R_{yz}} \\ F_{R_{yz}} & F_{R_{zz}} \end{pmatrix}^{-1}\begin{pmatrix} F_{R_{xy}} \\ F_{R_{xz}} \end{pmatrix}\right]_{i,i}^{-1} \\ &+ \left[F_{R_{yy}} - (F_{R_{xy}}F_{R_{yz}})\begin{pmatrix} F_{R_{xx}} & F_{R_{xz}} \\ F_{R_{xz}} & F_{R_{zz}} \end{pmatrix}^{-1}\begin{pmatrix} F_{R_{xy}} \\ F_{R_{yz}} \end{pmatrix}\right]_{i,i}^{-1} \\ &+ \left[F_{R_{zz}} - (F_{R_{xz}}F_{R_{yz}})\begin{pmatrix} F_{R_{xx}} & F_{R_{xy}} \\ F_{R_{xy}} & F_{R_{yy}} \end{pmatrix}^{-1}\begin{pmatrix} F_{R_{xz}} \\ F_{R_{yz}} \end{pmatrix}\right]_{i,i}^{-1} \end{aligned} \tag{9}$$

3.2 CRB for Capsule Localization with Randomness in Power

Here, the unknown parameters to be estimated is x, y and z coordinate of the capsules, and a new vector $\pi = [\pi_{01}, \ldots, \pi_{0N}]$ since none of the N sensors have perfect knowledge of their transmit power. The Bayesian CRB [21] also called as Van trees inequality states that any estimator $\hat{\theta}$ must have error correlation matrix $R_\in$ satisfying

$$R_\in > F^{-1} = [F_\theta + F_p] \tag{10}$$

where $R_{\in} = E[(\hat{\theta}-\theta)(\hat{\theta}-\theta)^T]$, with F_θ and F_p are the FIM and prior information matrix respectively and are give by Eq. 11

$$\begin{aligned} F_\theta &= -E\left[\bigtriangledown_\theta(\bigtriangledown_\theta \ln f(p_{i,j}|\theta))^T\right] \\ F_p &= -E[\bigtriangledown_\theta(\bigtriangledown_\theta \ln f(\theta))^T] \end{aligned} \tag{11}$$

where $p_{i,j}$ is the bi-directional measurement vector. The prior information matrix F_p is given in Eq. 12

$$F_p = diag\left[0_n^T, 0_n^T, 0_n^T, 1_N^T/\sigma_\pi^2\right] \tag{12}$$

where 0_n is a n-length vector of zeros and 1_N is an N length vector of ones and σ_π^2 is the variance of the random variable π_{0i} (the power at 1 cm distance from transmitter i) which is assumed to have an i.i.d Gaussian prior for every sensor i.

We model the bi-directional measurements $P_{i,j}$ and $P_{j,i}$ using vector $p_{i,j} = [P_{i,j}P_{j,i}]$ as a bi-variate gaussian with mean $u_{i,j}$ and variance $C_{i,j}$, where

$$u_{i,j} = \begin{bmatrix} \pi_{0j} - 10\alpha\log_{10}\frac{|ri-rj|^2}{\triangle_0^2} \\ \pi_{0i} - 10\alpha\log_{10}\frac{|ri-rj|^2}{\triangle_0^2} \end{bmatrix} \tag{13}$$

$$C_{i,j} = \sigma_{\mathrm{dB}}^2 \begin{bmatrix} 1 & \rho \\ \rho & 1 \end{bmatrix} \tag{14}$$

where α is the path loss exponent, and ρ is the correlation coefficient between the bidirectional measurements, $0 \le \rho \le 1$. For the purpose of discussion we transform the bidirectional measurement vector $p_{i,j}$ by an orthogonal matrix A as:

$$\tilde{p_{i,j}} = Ap_{i,j}, \quad A = \begin{bmatrix} 1 & 1 \\ 1 & -1 \end{bmatrix} \tag{15}$$

such a full rank transformation of measurement does not change the Fisher information. For simplicity of notation, we denote $\tilde{p}_{i,j} = [\bar{p}_{i,j}p_{ij}^{\triangle}]^T$, where $\bar{p}_{ij}$ corresponds to the average of the two measurements and $p_{ij}^{\triangle}$ corresponds to the difference between the two measurements. After some mathematical analysis, it is seen that $\bar{p}_{ij}$ has a mean $\bar{u}_{ij}$ and covariance $\bar{C}$ and $p_{ij}^{\triangle}$ has a mean $u_{ij}^{\triangle}$ and covariance $C^{\triangle}$ as given below:

$$\begin{aligned} \bar{u}_{ij} &= \pi_{0j} + \pi_{0i} - 10\alpha\log_{10}\frac{|ri-rj|^2}{\triangle_0^2}; \quad \bar{C} = \frac{(1+\rho)\sigma_{\mathrm{dB}}^2}{2} I_{3n+N} \\ u_{ij}^{\triangle} &= \frac{\pi_{0j}-\pi_{0i}}{2}; \quad C^{\triangle} = \frac{(1-\rho)\sigma_{\mathrm{dB}}^2}{2} I_{3n+N} \end{aligned} \tag{16}$$

where I_{3n+N} is $3n+N \times 3n+N$ identity matrix and $\bar{u}$ and $u^{\triangle}$ are the mean values of the sum and difference of measurements respectively for all measurement pairs,

$$\bar{u} = [\bar{u}_{i_1,j_1}, \ldots, \bar{u}_{i_s,j_s}]^T; \quad u^{\triangle} = [u_{i_1,j_1}^{\triangle}, \ldots, u_{i_s,j_s}^{\triangle}] \tag{17}$$

where $i_1, j_1, \ldots, i_s, j_s$ corresponds to each unique pair. A pair makes measurement if they are in the measurement range of each other. Here we assume that the measurement range is infinite (i.e., every sensor can do measurements with every other sensor). The Fisher information matrix F_θ given in Eq. 11 can be split into two sub matrices $\bar{F}_\theta$ and $F_\theta^{\triangle}$ corresponding to sum and difference measurements due to their independence.

$$F_\theta = \bar{F}_\theta + F_\theta^{\triangle} \tag{18}$$

The FIM of a vector of multivariate Gaussian measurements with mean $\mu(\theta)$ and covariance C is given by [17]

$$\begin{aligned} F_\theta &= [\bigtriangledown_\theta \mu(\theta)]^T C^{-1} [\bigtriangledown_\theta \mu(\theta)] \\ &= \begin{bmatrix} F_{Rxx} & F_{Rxy} & F_{Rxz} & F_{Rx\pi} \\ F_{Ryx} & F_{Ryy} & F_{Ryz} & F_{Ry\pi} \\ F_{Rzx} & F_{Rzy} & F_{Rzz} & F_{Rz\pi} \\ F_{R\pi x} & F_{R\pi y} & F_{R\pi z} & F_{R\pi\pi} \end{bmatrix} \end{aligned} \tag{19}$$

From Eq. 18, we have,

$$\bar{F}_\theta = [\bigtriangledown_\theta \bar{\mu}]^T C^{-1} [\bigtriangledown_\theta \bar{\mu}] = \begin{bmatrix} \bar{F}_{Rxx} & \bar{F}_{Rxy} & \bar{F}_{Rxz} & \bar{F}_{Rx\pi} \\ \bar{F}_{Ryx} & \bar{F}_{Ryy} & \bar{F}_{Ryz} & \bar{F}_{Ry\pi} \\ \bar{F}_{Rzx} & \bar{F}_{Rzy} & \bar{F}_{Rzz} & \bar{F}_{Rz\pi} \\ \bar{F}_{R\pi x} & \bar{F}_{R\pi y} & \bar{F}_{R\pi z} & \bar{F}_{R\pi\pi} \end{bmatrix} \tag{20}$$

$$\begin{aligned} \bar{F}_\theta^{\triangle} &= [\bigtriangledown_\theta \mu^{\triangle}]^T C^{-1} [\bigtriangledown_\theta \mu^{\triangle}] \\ &= \begin{bmatrix} \bar{F}_{Rxx}^{\triangle} & \bar{F}_{Rxy}^{\triangle} & \bar{F}_{Rxz}^{\triangle} & \bar{F}_{Rx\pi}^{\triangle} \\ \bar{F}_{Ryx}^{\triangle} & \bar{F}_{Ryy}^{\triangle} & \bar{F}_{Ryz}^{\triangle} & \bar{F}_{Ry\pi}^{\triangle} \\ \bar{F}_{Rzx}^{\triangle} & \bar{F}_{Rzy}^{\triangle} & \bar{F}_{Rzz}^{\triangle} & \bar{F}_{Rz\pi}^{\triangle} \\ \bar{F}_{R\pi x}^{\triangle} & \bar{F}_{R\pi y}^{\triangle} & \bar{F}_{R\pi z}^{\triangle} & \bar{F}_{R\pi\pi}^{\triangle} \end{bmatrix} \end{aligned} \tag{21}$$

The derivation of the individual elements of the matrix are similar to Eq. 8, and given in [22].

4 Simulation Results

4.1 Setup

The simulation setup is based on the application of WCE requiring localization of capsule in stomach, small intestine and large intestine environments. Esophagus is not included as a simulation scenario because traditional upper endoscopy techniques are powerful enough to diagnose diseases in it. M receiver sensors are distributed evenly on the surface of the body torso, see Fig. 3. N capsule pills are then distributed inside the GI tract environment. Connectivity is assumed between capsule pills and the receiver sensors and among capsule pills. The path loss parameters are determined by the length of each connection as mentioned in Sect. 2.

For the analysis of the simulations, we compute the average RMS of the location error of each situation. For the

case of N different capsule locations, the RMSE is computed by:

$$RMSE = \frac{\sqrt{\sum_{i=1}^{N} \sigma_{x_i}^2 + \sigma_{y_i}^2 + \sigma_{z_i}^2}}{N} \quad (22)$$

where $\sigma_{x_i}^2, \sigma_{y_i}^2$, and $\sigma_{z_i}^2$ are the variance of each coordinate value of the ith pill location.

4.2 Effect of Organ Shape and Location

In this section, we evaluate the impact of the organ shape and location on localization accuracy. For the simulation, we fixed the number of receiver sensors to 32 and assumed only one single capsule in each organ. We calculated the 3D-CRB for all the possible location points inside each organ (634 points for stomach, 1,926 points for small intestine and 3,334 points for large intestine). Figure 5 shows the CDF comparison of location error bound in different organs.

Notice that the localization error for capsule in small intestine is apparently smaller than that in large intestine. The average value of σ_{error} for small intestine environment is 45.5 mm, while it is 49 mm for large intestine environment. The localization error for capsule in stomach has the lowest average value but distributed in a wider range compared to the errors in other two environments. These observations can be explained by the geometric relationship between the sensor array and the organs. As we can see from Fig. 4, stomach is located in the upper part of the receiver sensor array system, and its volume is the smallest among the three organs. Therefore, the localization error varies more in the stomach environment. The points located in the upper part of stomach have larger localization error value as they are far from the center of the receiver array system, the points in the lower part of stomach have smaller localization error value. The small intestine is located in the center part of human abdomen cavity and the lumen is more centralized compared to large intestine. Therefore, the localization error inside small intestine is smaller than that in large intestine.

4.3 Effect of Number of Receiver Sensors

In this section, we investigate the impact of number of receiver sensors on localization accuracy. In this experiment, 12,000 Monte Carlo simulations (3 different organs, 4 different number of receiver sensors and 1,000 simulations per organ) were carried out with the number of receiver sensors varied from 8 to 64. During each simulation, we assume one capsule is located randomly inside each organ. The results show that the number of receivers has significant influence on the accuracy of localization when the number of receivers is smaller than 32. The localization accuracy in small intestine is less sensitive to the number of receivers. This means that large intestine and stomach are harsher implant environments for RF localization which requires more receiver sensors on body surface to achieve similar localization performance as environments with better geometric and channel condition. Finally, notice that for all the three organs, at least 32 receiver sensors are needed to guarantee the performance of 50 mm average RMSE (Fig. 6).

4.4 Effect of Sensor Configuration

In this simulation, three different sensor placement for receiver sensors are considered which represents the potential sensor arrangement in practice as shown in Fig. 7.

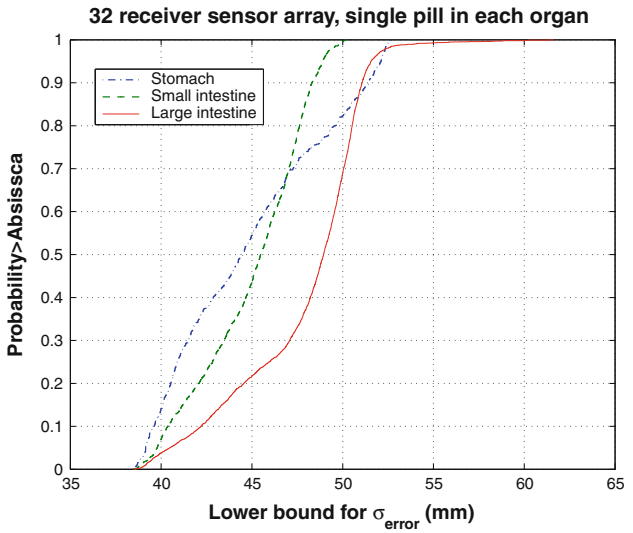

Fig. 5 CDF comparison of location error bound in stomach, small intestine and large intestine

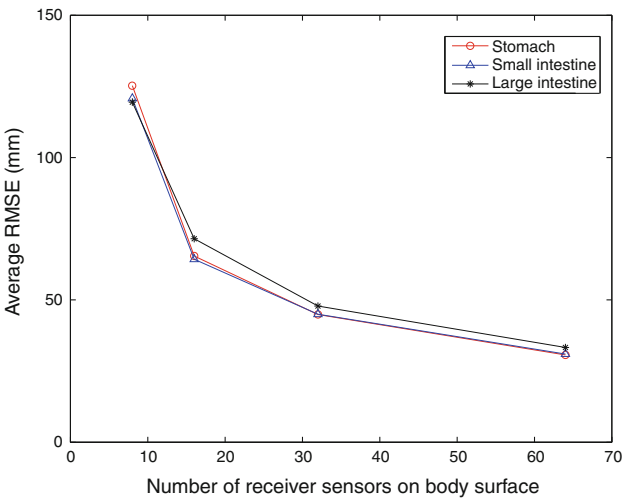

Fig. 6 Localization performances as a function of number of receiver sensors in different organs

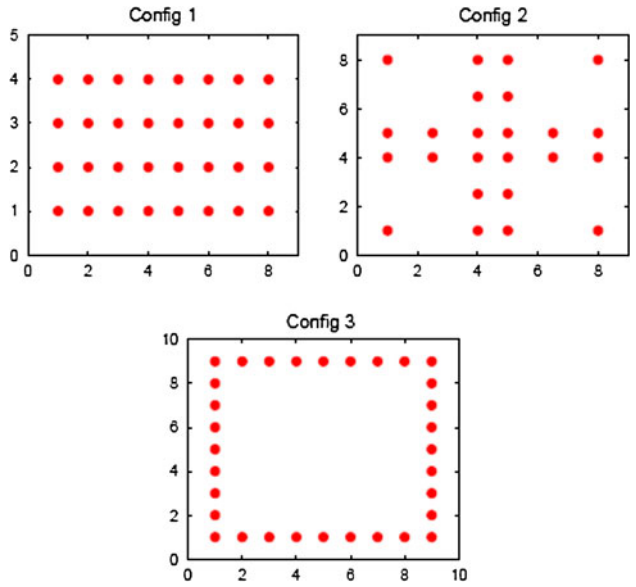

Fig. 7 Three sensor configuration considered for analysis of the bounds (number of sensors = 64)

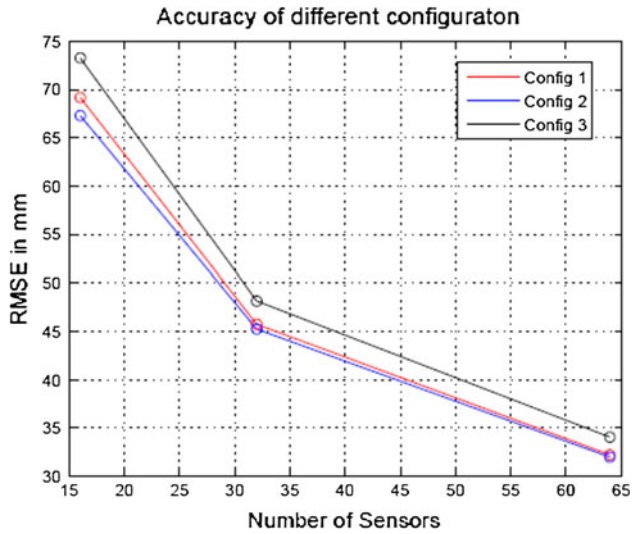

Fig. 8 Three sensor configuration considered for analysis of the bounds (number of sensors = 64)

Half of the sensors are on the front plane of the jacket and half of them are in the rear plane of the jacket. These sensor configurations can be seen to have three distinct forms namely, Config1: sensors uniformly distributed in both the planes of the jacket, Config2: sensors concentrated at the center of the jacket, and Config3: sensors concentrated at the borders of the jacket. Figure 8 shows the RMSE of the three different sensor population for all three configurations. It can be observed that better performance is achieved when the sensors are concentrated near the center of the jacket. Arranging all the sensors concentrating on the boundary should be avoided since such configuration performs the worst.

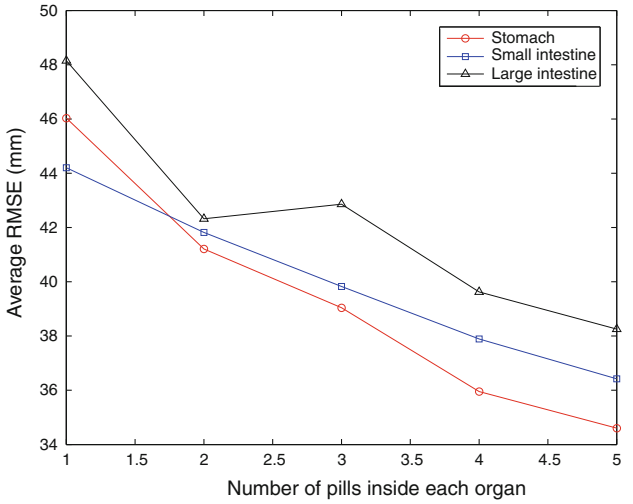

Fig. 9 Localization performances as a function of number of pills in different organs

4.5 Effect of Number of Pills in Cooperation

Next, we investigate the impact of cooperation among pills. For this simulation, we fixed the number of receivers on body surface to 32 and increased the number of pills from 1 to 5. The pills are assumed to be randomly distributed inside each organ and they can measure the RSS from each other. 15,000 simulations were carried out to study the effect of cooperation among pills. The results are presented in Fig. 9. It is shown that as the number of pills increase from 1 to 5. The localization accuracy in all three organs improved, especially for large intestine and stomach environments. Localization accuracy in small intestine is again less sensitive to the number of pills which means it is a lighter environment for RF propagation and geometrically better surrounded by the receiver array. Notice that in practical situations, we do not want to send a lot of capsules into a patient due to the potential danger of digestion disorder and uncomfort for patient. Compared to the impact of number of receiver sensors, the number of pills in cooperation has less influence on the accuracy of localization. Therefore, our results indicate that increasing the number of receiver sensors on body surface is a more effective way to improve the overall localization performance than increasing the number of pills in cooperation for RSS based capsule localization.

4.6 Effect of Random Power on the Bounds in Different Organs

In this section, we calculate the bounds for different organs when there's randomness in the transmitted power. We plot the lower bound on the $1 - \sigma$ uncertainty ellipse for $\hat{r}_i$, the estimate of the ith capsule sensor coordinate. In this example, we use $\sigma_{\text{dB}} = 7.85$ and $\alpha = 4.26$ based on the path loss model

Table 2 Percentage increase in the RMSE (mm) of the capsule in three different organs of the GI track

Human organ	$\sigma_\pi = 0$ dB	$\sigma_\pi = 10$ dB	%
Stomach	20.8284	21.8090	4.7
Small intestine	22.1399	22.4024	1.2
Large Intestine	26.2381	28.0591	7.1

discussed in Sect. 2. For the simulation, we consider $\rho = 0.704$. The bounds behaves similar at different values of ρ. We also found the bounds as a function of ρ. Finally, in these examples, the prior knowledge of transmit power is $\sigma_\pi = 10$ dB. We also consider the case when $\sigma_\pi = 0$ dB for comparison purpose.

For perfectly known transmit power (i.e. $\sigma_\pi = 0$ dB), the uncertainty ellipse is shown by solid lines whereas for $\sigma_\pi = 10$ dB, it is shown by dotted lines. As we can see in Table 2, the increase in the RMSE for all three organs when, randomness in the transmit power exist.

Figure 2 shows corresponding bound in each organ individually. It is observed with given configuration of anchor nodes capsules in large intestine suffered the largest localization error when there was variance in transmit power. For small intestine, the value of RMSE for $\sigma_\pi = 0$ dB was 22.1399 mm and for $\sigma_\pi = 10$ dB was 22.4024 mm.

4.7 Performance as a Function of σ and ρ

Next, we calculate the bound over the entire range of correlation coefficient values. Here, we have used a grid of 64 sensors with configuration number 3. The rest of the parameters are kept the same as the previous simulations. In this experiment, the capsule is assumed to be in any one of the three organs and the average performance bounds as a function of ρ is calculated. As seen in Fig. 10, as $\rho \to 1$ the lower bounds are not affected with randomness in transmitted power as much as it is affected at lower value of ρ. Also, at lower values of ρ, the RMSE is lower than that at the higher values.

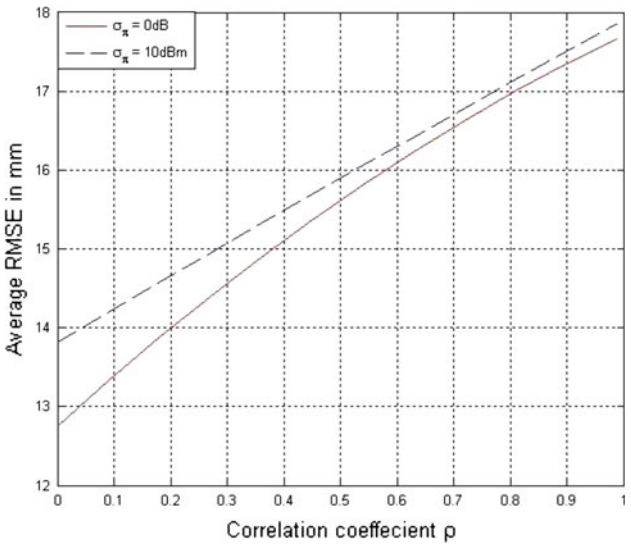

Fig. 10 CRB for σ_r for 64 sensor configuration for two values of σ_π and a range of *rho* ($\sigma_{\text{dB}} = 7.85$ and $\alpha = 4.26$)

5 Conclusion

In this paper, we investigated the potential accuracy limit for RSS triangulation based capsule localization in the human GI tract. We verified the possibility of achieving average localization error 50 mm in the digestive organs. We also verified that more than 32 sensors on body surface is needed for achieving satisfying localization accuracy for capsule endoscopy. Simulation results showed that increasing the number of receiver sensors on body surface has more influence of the overall localization performance than increasing the number of pills inside the GI tract. We also analyzed the effect of randomness in transmit power on the localization accuracy. Considering the practical issues, we draw the conclusion that increasing the number of receiver sensors is a better way for reaching higher accuracy for capsule localization.

Acknowledgments The authors would like to express their acknowledgements to Dr.Kaveh Ghaboosi, Umair Khan, Ruijun Fu, Dr. Nayef Alsindi and other colleagues in CWINS lab in preparing of this paper. And the National Institute of Science and Technology (NIST) for funding support on this paper.

References

1. J. Oh, S. K. Shah, X. Yuan, and S. J. Tang, Automatic classification of digestive organs in wireless capsule endoscopy videos, In *The 22nd Annual ACM Symposium on Applied Computing, SAC07*, Soul, 2007.
2. M. Frisch, A. Glukhovsky, and D. Levy, Array system and method for locating an in vivo signal source, Patent US2002/0 173 718, May 20, 2002.
3. M. Fischer, R. Schreiber, D. Levi, and R. Eliakim, Capsule endoscopy: the localization system, *Gastrointestinal Endoscopy Clinics of North America*, Vol. 14, pp. 25–31, 2004.
4. J. R. R. Kuth and R. Rockelein, Method for determining the position and orientation of an endoscopy capsule guided through an examination object by using a navigating magnetic field generated by means of a navigation device, Patent, February 15, 2007.
5. M. Kawasaki and R. Kohno, A TOA based positioning technique of medical implanted services, In *Third International Symposium on Medical Information & Communication Technology, ISMCIT09*, Montreal, 2009.
6. M. Q. M. Chao Hu and M. Mandal, Efficient magnetic localization and orientation technique for capsule endoscopy, In *Intelligent Robots and Systems, 2005. (IROS 2005)*, 2005.
7. A. M. Gastone Ciutia, P. Valdastria, and P. Darioa, Robotic magnetic steering and locomotion of microsystems for diagnostic and surgical endoluminal procedures, In *Robotica*, 2009.
8. S. Thomas, Smartpill redefines 'noninvasive', *Buffalo Physician*, Vol. 40, pp. 13–14, 2006.
9. J. H. D. Levy, R. Shreiber, A. Glukhovsky, and D. Fisher, Localization of the given M2A ingestible capsule in the given diagnostic imaging system *Gastrointestinal Endoscopy*, Vol. 55, p. AB135, 2002.

10. L. Wang, C. Hu, L. Tian, M. Li, and M. Q. H, A novel radio propagation radiation model for localization of the capsule in GI tract, In *IEEE International Conference on Robotics and Biomimetics*, December 19–23, 2009.
11. K. Arshak and F. Adepoju, Adaptive linearized methods for tracking a moving telemetry capsule, In *IEEE International Symposium on Industrial Electronics (ISIE)*, June 2007, pp. 4–7.
12. K. Sayrafian-Pour, W.-B. Yang, J. Hagedorn, J. Terrill, and K. Yazdandoost, A statistical path loss model for medical implant communication channels, In *2009 IEEE 20th International Symposium on Personal, Indoor and Mobile Radio Communications*, 13–16 September 2009, pp. 2995–2999.
13. Y. Wang, R. Fu, Y. Ye, K. Umair, and K. Pahlavan, Performance bounds for RF positioning of endoscopy camera capsules, In *IEEE Radio and Wireless Week*, Phoenix, Arizona, 2011.
14. N. Alsindi and K. Pahlavan, Cooperative localization bounds for indoor ultra-wideband wireless sensor networks, *EURASIP Journal on Advances in Signal Processing*, Vol. 2008, pp. 125:1–125:13, January 2008. doi:10.1155/2008/852509.
15. N. Bargshady, K. Pahlavan, Y. Ye, F. Akgul, and N. Alsindi, Bounds on performance of hybrid WiFi-UWB cooperative localization for robotic applications, In *Proceedings of IEEE International Symposium on Personal, Indoor and Mobile Radio Communications (PIMRC10)*, 2010.
16. Ansoft Full-wave electromagnetic field simulation, http://www.ansoft.com/products/hf/hfss/, Online; accessed 27 September 2010.
17. N. Patwari and A. Hero, Signal strength localization bounds in ad hoc and sensor networks when transmit powers are random, In *Fourth IEEE Workshop on Sensor Array and Multichannel Processing, 2006*, July 2006, pp. 299–303.
18. K. Y. Y. H.-B. Li and B. Zhen, *Wireless body area network*. River Publishers, 2010.
19. N. Patwari, I. Hero, A.O., M. Perkins, N. Correal, and R. O'Dea, Relative location estimation in wireless sensor networks, In *IEEE Transactions on Signal Processing*, August 2003, pp. 2137–2148.
20. J. Bulat, K. Duda, M. Duplaga, R. Fraczek, A. Skalski, M. Socha, P. Turcza, and T. Zielinski, Data processing tasks in wireless GI endoscopy: image-based capsule localization and navigation with video compression, In *Proc. of IEEE/EMBS*, 2007, pp. 2815–2818.
21. H. L. V. Trees, *Detection, Estimation, and Modulation Theory: Part I*, Wiley, New York, 1968.
22. K. G. P. Swar, Y. Ye, and K. Pahlavan, On effect of transmit power variance on localization accuracy in wireless capsule endoscopy, In *IEEE Wireless Communications and Networking Conference (WCNC 2012)*, Paris, 2012.

Author Biographies

Yunxing Ye is a Ph.D. student under the guidance of Professor Kaveh Pahlavan in the Electrical Engineering Department at Worcester Polytechnic Institute. He received the B.S. degrees in Electrical Engineering from Zhejiang University, Hangzhou, China and M.S. degree in Electrical and Computer Engineering from Worcester Polytechnic Institute. His current research interests include Cooperative robot localization and Body area network (BAN).

Pranay Swar is a M.S. student in the Department of Electrical and Computer Engineering at Worcester Polytechnic Institute (W.P.I), Worcester, MA. He received his B.E. degree in Electronics and Telecommunication form University of Mumbai, Mumbai, India. His current research interest include Body Area Networks.

Kaveh Pahlavan is a professor of Electrical and Computer Engineering, a Professor of Computer Science, and Director of the Center for Wireless Information Network Studies, Worcester Polytechnic Institute, Worcester, Massachusetts and the chief technical advisor of Skyhook Wireless, Boston, Massachusetts. His current area of research is opportunistic localization for body area networks and robotics applications. He is the principal author of Wireless Information Networks (with Allen Levesque), John Wiley and Sons, 1995, 2ed Ed. 2005; Principles of Wireless Networks—A Unified Approach (with P. Krishnamurthy), Prentice Hall, 2002; and Networking Fundamentals: Wide, Local, and Personal Communications (with P. Krishnamurthy), Wiley 2009. He is the founder and editor-in-chief of the International Journal on Wireless Information Networks and founder and chairman of a number of IEEE conferences in wireless access and localization. He was awarded Westin Hadden Professor of ECE at WPI during 1993–1996, elected as a fellow of IEEE in 1996, awarded a Nokia fellowship in 1999, and the first Fulbright-Nokia scholar at University of Oulu, Finland, 2000.

Kaveh Ghaboosi received his B.Sc. on Electrical Engineering—Control Systems from University of Tehran, Iran, in 2002 (with honor), and his M.Sc. on Electrical Engineering—Wireless Communications Systems from Sharif University of Technology, Tehran, Iran, in 2004. He also received his Ph.D. degree from Centre for Wireless Communications (CWC), University of Oulu, Finland, under Nokia and Nokia Siemens Networks sponsorship in October 2009, where his thesis was nominated as the best Ph.D. thesis in Finland. He did half of his Ph.D. degree program at Virginia Tech for approximately one year under supervision of Professor Allen B. MacKenzie. He was also a Post-doctoral Research Fellow at the University of Oulu until September 2010 when he moved to the United States and began working at Worcester Polytechnic Institute (WPI) as a Post-doctoral Research Fellow under Professor Kaveh Pahlavan's supervision. He joined Airvana on July 18, 2011, where he works in LTE Femtocell group.